PNAS RESEARCH ARTICLE | CELL BIOLOGY

Leading-edge elongation by follower cell interruption in advancing epithelial cell sheets

Chika Okimura [a], Misaki Iwanaga[a], Tatsunari Sakurai[b], Tasuku Ueno[c], Yasuteru Urano [c,d], and Yoshiaki Iwadate[a,1]

Edited by Alex Mogilner, New York University, New York, NY; received November 1, 2021; accepted March 21, 2022 by Editorial Board Member Yale E. Goldman

Collective cell migration is seen in many developmental and pathological processes, such as morphogenesis, wound closure, and cancer metastasis. When a fish scale is detached and adhered to a substrate, epithelial keratocyte sheets crawl out from it, building a semicircular pattern. All the keratocytes at the leading edge of the sheet have a single lamellipodium, and are interconnected with each other via actomyosin cables. The leading edge of the sheet becomes gradually longer as it crawls out from the scale, regardless of the cell-to-cell connections. In this study, we found leading-edge elongation to be realized by the interruption of follower cells into the leading edge. The follower cell and the two adjacent leader cells are first connected by newly emerging actomyosin cables. Then, the contractile forces along the cables bring the follower cell forward to make it a leader cell. Finally, the original cables between the two leader cells are stretched to tear by the interruption and the lamellipodium extension from the new leader cell. This unique actomyosin-cable reconnection between a follower cell and adjacent leaders offers insights into the mechanisms of collective cell migration.

actomyosin cable | collective cell migration | lamellipodium

Significance

Collective cell migration is an important phenomenon in the developmental process of living organisms and even in mature individuals. The cells in the collective are accurately classified into leader cells, which lead the collective at the leading edge, and follower cells. We found that in the collective migration of keratocytes, the epidermal cells of fish responsible for wound repair, a mechanical interaction between two leader cells and a single follower cell can forcibly break the connection between the two leader cells and transform the follower cell into a leader cell.

In multicellular organisms, collective cell migration plays a key role in many developmental and pathological processes, such as morphogenesis, wound closure, and cancer metastasis (1, 2). Collective coordinated movements of epithelial cells drive not only wound closure but also morphogenesis, such as dorsal closure during *Drosophila* embryogenesis.

It appears that two main mechanisms contribute to epithelial gap closure: 1) formation of intracellular actomyosin cables surrounding the gap margin and their contraction in a purse-string manner, and 2) cell crawling migration driven by lamellipodial and/or filopodial protrusions. Gap closure by the contraction of an actomyosin "purse string" was first shown in chicken embryos (3), and subsequently in other contexts, such as *Drosophila* embryos (4), *Xenopus* embryos (5), Madine-Darby canine kidney (MDCK) cell culture (6), and keratinocytes (7). In many cases—such as repair of artificial circular wounds in intestinal epithelia (8), *Drosophila* embryos (9), murine corneal epithelia (10), bovine corneal epithelia (11), MDCK cells (12, 13), dorsal closure of *Drosophila* embryos (14, 15), and cranial neural tube closure of mouse embryos (16)—cells exhibit not only the actomyosin purse-string behavior but also cellular protrusions at their leading edge, indicating that cells undergoing collective migration can combine both mechanisms to enable them to move.

The classic scratch wound assay is a standard in vitro technique for probing collective cell migration in two dimensions (17). In this assay, a confluent epithelium is scratched with a pipette or a razor blade to make a linear thin scratch wound in a confluent cell monolayer. Model wound assays are increasingly being used (18–20). In this assay, obstacles are placed on the preproliferation substrate to prevent scratch damage to the cell sheet. The obstacles are then removed after the cells have become confluent. Some cells at the edges of scratches or model wounds transform into crawling "leader" cells that possess a large forward lamellipodium (19, 21–23) and begin to advance with other cells that act as "follower" cells. The assembly of supracellular actomyosin cables is frequently observed between two leader cells, and this would appear to prevent new leader cell formation (12, 24–27) due to the mechanical stress produced by the contraction of actomyosin cables (28). These cables are reminiscent of those observed in the purse-string process.

Recently, Wei et al. (29) found a novel actomyosin cable-switching mechanism in nonadhesive gap closure by MDCK cells, in which a follower cell closest to the leader cells is pushed into the gap front by the cell-proliferative pressure of posterior follower cells, and an original leader cell moves behind the new leader cell. Actin fibers in the new leader cell fuse into the actomyosin cables, and those from the original leader cell

Author affiliations: [a]Department of Biology, Yamaguchi University, Yamaguchi 753-8512, Japan; [b]Department of Mathematical Engineering, Musashino University, Tokyo 135-8181, Japan; [c]Graduate School of Pharmaceutical Sciences, The University of Tokyo, Tokyo 113-0033, Japan; and [d]Graduate School of Medicine, The University of Tokyo, Tokyo 113-0033, Japan

Author contributions: C.O. and Y.I. designed research; C.O., M.I., T.S., T.U., Y.U., and Y.I. performed research; T.U. and Y.U. contributed new reagents/analytic tools; C.O., M.I., T.S., and Y.I. analyzed data; and C.O. and Y.I. wrote the paper.

The authors declare no competing interest.

This article is a PNAS Direct Submission. A.M. is a guest editor invited by the Editorial Board.

Copyright © 2022 the Author(s). Published by PNAS. This article is distributed under Creative Commons Attribution-NonCommercial-NoDerivatives License 4.0 (CC BY-NC-ND).

[1]To whom correspondence may be addressed. Email: iwadate@yamaguchi-u.ac.jp.

This article contains supporting information online at http://www.pnas.org/lookup/suppl/doi:10.1073/pnas.2119903119/-/DCSupplemental.

Published April 27, 2022.

defuse. This mechanism is different from the classic gap-closure mechanism where cell proliferation contributes negligibly to the gap closure (7) and actin fiber fusion/defusion is absent.

When fish skin receives an injury, epithelial keratocyte sheets migrate to repair the wound (30). Single-cell keratocyte systems have been used in many studies of cell motility because of their constant cell shape during their high-speed (>10 μm/min) movement (31–34). Keratocytes are not only a powerful tool for studying single-cell motility, but they could potentially be used to study the collective migration of epithelial cell sheets. When a scale removed from a fish is attached to a substrate, such as a coverslip, keratocyte collectives crawl out from the scale-skin onto the surface of the substrate (35). The epithelial keratocyte sheets crawling out of the scales show a semicircular pattern. All the keratocytes at the front row (leading-edge cells) have polarized lamellipodia that are characteristic of leader cells (36). At the same time, actomyosin cable segments are distributed at the lamellipodium cell-body boundary in each leader cell, and are interconnected with each other via cell-to-cell adhesion containing vinculin (36, 37). This architecture is similar to the actomyosin purse string. Normally, the gaps surrounded by the actomyosin purse string shrink as a result of its contraction. On the other hand, it is noteworthy that the leading edges of the keratocyte sheets gradually become longer as they crawl out from the scale, regardless of cell-to-cell connections by actomyosin cables.

In this study, we will show the unique interaction of follower cells with their neighboring two leader cells that enable elongation of the leading edge. New actomyosin cables connect between a follower cell and the neighboring two leader cells. Contractile forces of them bring the follower cell ahead, and the follower cell extends its lamellipodium, by which the original actomyosin cables between the two leader cells are broken, and the follower cell transforms to a leader cell. This is similar to the actomyosin cable-switching mechanism by Wei et al. (29); however, it differs in the following ways: It is driven not by the posterior cell-proliferative pressure but by the mechanical interaction between a follower cell and the neighboring two leader cells; original cables between the two leader cells break without fusing with the actin fibers in the interrupting follower cell; and the leader cells never transform to follower cells. This actomyosin cable dynamic system and the interaction between leader and follower cells reveals information on collective cell migration.

Results

Leading Edges of Keratocyte Sheets Become Longer during Their Advance. When a scale is taken from an African cichlid (*Maylandia lombardoi*) and attached to a coverslip, epithelial keratocytes that are taken along with the scale begin to crawl out collectively as a sheet from the scale within a few minutes of attaching the scale (Movie S1). During collective migration (Fig. 1*A*), multiple leader cells advance while extending their lamellipodia (Fig. 1*B*), followed by a large number of follower cells (35, 36, 38). As the keratocyte sheet crawls out of the scale, the leading edge of the sheet appears to elongate (3 h in Fig. 1*A*). To confirm this possibility, we measured the time courses of the length between the two arbitrarily selected leader cells in the leading edge of the keratocyte sheets (*a* and *b* in Fig. 1*A*). In all 11 sheets, the length of the leading edge clearly increased as the sheet advanced (Fig. 1*C*).

In the Cell Sheets, Each Cell Extends a Cryptic Pseudopod under the Cell Ahead. It has previously been reported that leader cells of keratocyte sheets have purse-string–like actomyosin cables at the boundary between the lamellipodium and the cell body (36, 37). Actomyosin cables appear to be structurally and mechanically connected via cell-to-cell adhesions containing vinculin in adjacent leader cells. To clarify the details of keratocyte sheet architecture, we fixed the advancing sheets and stained filamentous actin (F-actin) with Alexa 488 phalloidin and simultaneously with myosin IIA (Fig. 1 *D* and *E*) or vinculin (Fig. 1 *I* and *J*) using immunofluorescent staining. Images taken by confocal microscopy are shown at the bottom (Fig. 1 *D* and *I*) and middle (Fig. 1 *E* and *J*) optical sections. Every sheet had a different thickness. Thus, the height of the middle section was defined as the height at which F-actin bundles (asterisks in Fig. 1 *E* and *J*) could be detected between the lamellipodium and the cell body in the leader cells. The heights of the middle images (Fig. 1 *E* and *J*) from the bottom (Fig. 1 *D* and *I*) are, respectively, 0.8 and 1.4 μm.

In the bottom section (Fig. 1 *D*, *Left*), not only in the leader cells but also in the follower cells, F-actin was detected in the anterior region of the cells. In the middle section, accumulation of F-actin was observed at the boundary between the lamellipodium and the cell body of leader cells (asterisk in Fig. 1 *E*, *Left*). F-actin also accumulated at the contours of cells in both the bottom and the middle sections (*Left* in Fig. 1 *D* and *E*).

For ease of observation of the three-dimensional connections of the cells that make up the sheet, the bottom areas of the four connected cells (Fig. 1 *D*, *a–d*, *Left*) are shown in different colors (Fig. 1*F*), and the contours of the same cells at the middle section (Fig. 1 *E*, *a–d*, *Left*) are drawn overlapped in the same colors as the bottom areas (Fig. 1*F*). In all four cells, the colored bottom area has moved ahead of the middle contour in the direction of migration. Next, perpendicular optical sections of F-actin images along the long axis of the rectangles in Fig. 1*D* were made (Fig. 1*G*). Constructed images were averaged along the short axis of each rectangle. The bottom F-actin in each cell (arrowheads in Fig. 1*G*) lies beneath the upper F-actin in the anterior cell (yellow arrows in Fig. 1*G*). These results clearly show that follower cells in keratocyte sheets extend cryptic lamellipodia into the bottom of the anterior cells (Fig. 1*H*), as also seen in other epithelial cell types (39).

The Actomyosin Cables in the Leader Cells are Connected via Cell-to-Cell Adhesions Containing Vinculin. In the bottom optical section (Fig. 1*D*), myosin IIA (Fig. 1 *D*, *Center*) was found in the lamellipodia of leader cells and in the cryptic lamellipodia of follower cells, as was F-actin (Fig. 1 *D*, *Left*). The colocalization of F-actin and myosin IIA can be seen (white in Fig. 1 *D*, *Right*). In the middle optical section (Fig. 1*E*), myosin IIA (Fig. 1 *E*, *Center*) was colocalized with F-actin at the boundary between the lamellipodium and the cell body of leader cells (yellow arrowheads in Fig. 1 *E*, *Right*), suggesting the presence of actomyosin cables. In both optical sections, F-actin fluorescence was strongly detected at the cell-to-cell boundaries, but myosin IIA was not (white arrowheads, *Center*, in Fig. 1 *D* and *E*).

Vinculin was also shown in the lamellipodia in leader cells in the bottom optical section (Fig. 1 *I*, *Center* and *Right*). In the middle optical section (Fig. 1*J*), vinculin was localized at the cell-to-cell boundary on the actomyosin cables (white arrowheads in Fig. 1 *J*, *Center* and *Right*), indicating that actomyosin cables are aligned in individual leader cells and are connected via cell-to-cell adhesions containing vinculin, as has been shown in previous studies (36, 37). Vinculin was also colocalized with F-actin at the contour of follower cells (yellow arrowheads in Fig. 1 *J*, *Center* and *Right*). To clarify the nature of the vinculin-labeled cell-to-cell junctions, we stained vinculin and

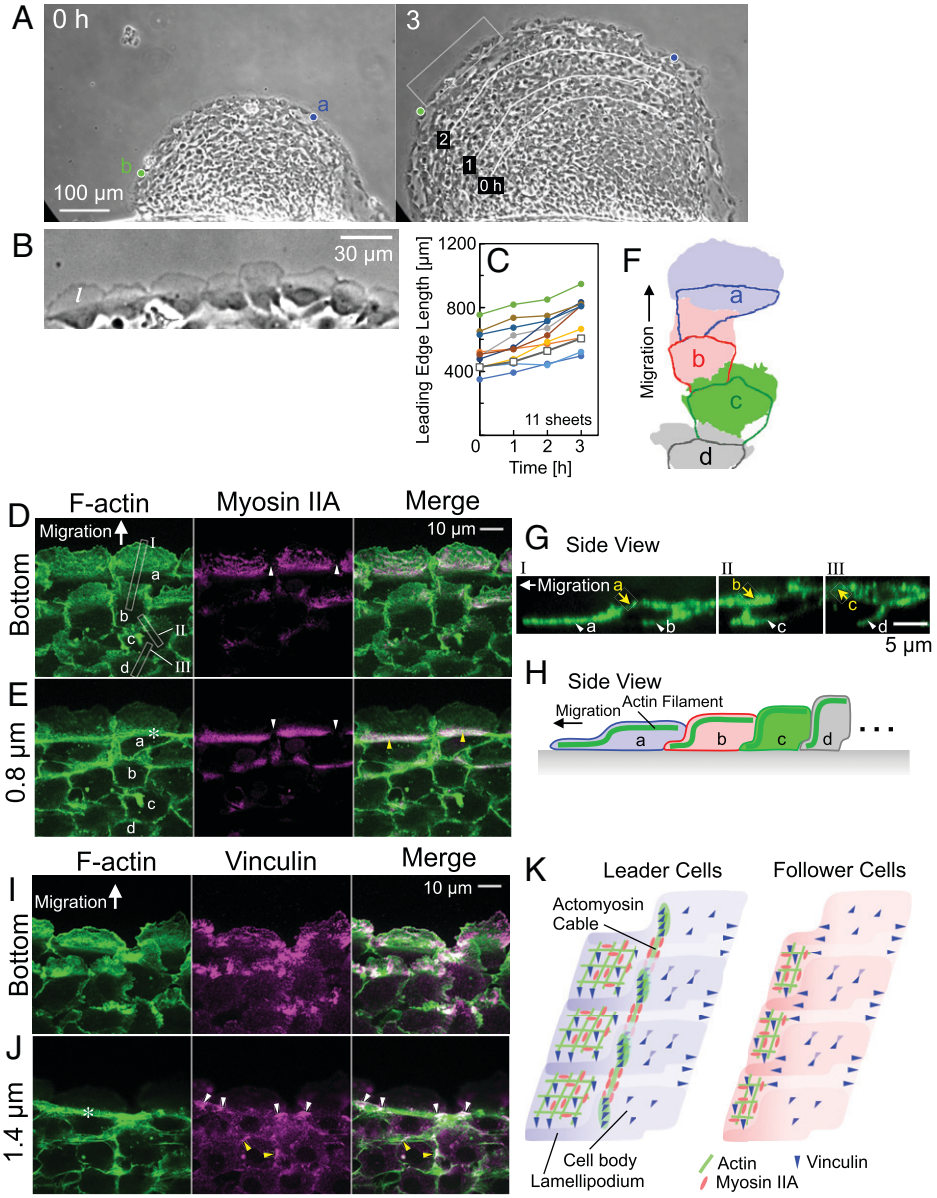

Fig. 1. Characteristics of keratocyte sheets migration and structure. (*A*) Sequential images of a migrating sheet. The *a* and *b* are two arbitrarily selected leader cells. Leading edges between *a* and *b* are drawn with white lines at each time (*Right*). Images in *A* are typical of 11 sheets. (*B*) Enlarged image of the rectangle in *A*, *Right*. Every leader cell has a lamellipodium (*l*). (*C*) Time courses of leading-edge lengths from 11 sheets. The data in *A* is represented by squares. In all cases, the leading edges became longer. (*D* and *E*) Bottom (*D*) and middle (*E*, 0.8 μm above the bottom) optical sections of a fixed keratocyte sheet. F-actin (green) and myosin IIA (magenta). Areas of colocalization of F-actin and myosin IIA appear white (*Right*). An asterisk represents accumulation of F-actin at the boundary between the lamellipodium and the cell body of leader cells. Yellow arrowheads: colocalization of F-actin and myosin IIA as actomyosin cables. White arrowheads: no myosin IIA at the cell-to-cell adhesions of actomyosin cables. Images in *D* and *E* are typical of 10 sheets. (*F*) The bottom areas of the four connected cells (*a–d* in *D*, *Left*) and the contours of the cells in the middle section (*a–d* in *E*, *Left*). The same cells are drawn in the same colors. (*G*) Perpendicular optical sections of F-actin images along the long axis of rectangles *I–III* in *D*. Constructed images from the data acquired by confocal microscopy were averaged along the short axis of the rectangles. (*H*) Side-viewed schematic illustration of a keratocyte sheet based on *F* and *G*. (*I* and *J*) Bottom (*I*) and middle (*J*, 1.4 μm above the bottom) optical sections of a fixed keratocyte sheet. F-actin (green) and vinculin (magenta). The asterisk represents actomyosin cables. White arrowheads: vinculin localization at the cell-to-cell boundary on the actomyosin cables. Yellow arrowheads: vinculin colocalization with F-actin at the contour of follower cells. Images in *I* and *J* are typical of 12 sheets. (*K*) Three-dimensional schematic illustration of the leader and follower cells in a keratocyte sheet based on *D–J*.

simultaneously with β-catenin or E-cadherin using immunofluorescent staining (*SI Appendix*, Fig. S1). β-Catenin was colocalized with vinculin at the cell-to-cell adhesions, but E-cadherin was not. The cell-to-cell adhesions connecting actomyosin cables may be slightly different from well-known adherens junctions. The structure of the keratocyte sheets obtained from these observations is summarized in schematic illustrations (Fig. 1*K* and Movie S2). It is an interesting question as to how the leading edge of keratocyte sheets becomes longer despite the leader cells being tightly connected to each other.

The Area Size of Leader Cells and Subsequent Follower Cells Remain Constant during Leading-Edge Elongation. The logical way to elongate the leading edge should be to increase the area or the number of leader cells. We first examined the former possibility. If the area size of the cells rises during collective cell migration, the internuclear distance between adjacent cells should simultaneously increase.

We stained the nuclei in each cell in the advancing sheets with DRAQ5 (Fig. 2 *A* and *B*) and recorded four sequential epi-fluorescence images of the nuclei every hour. The time

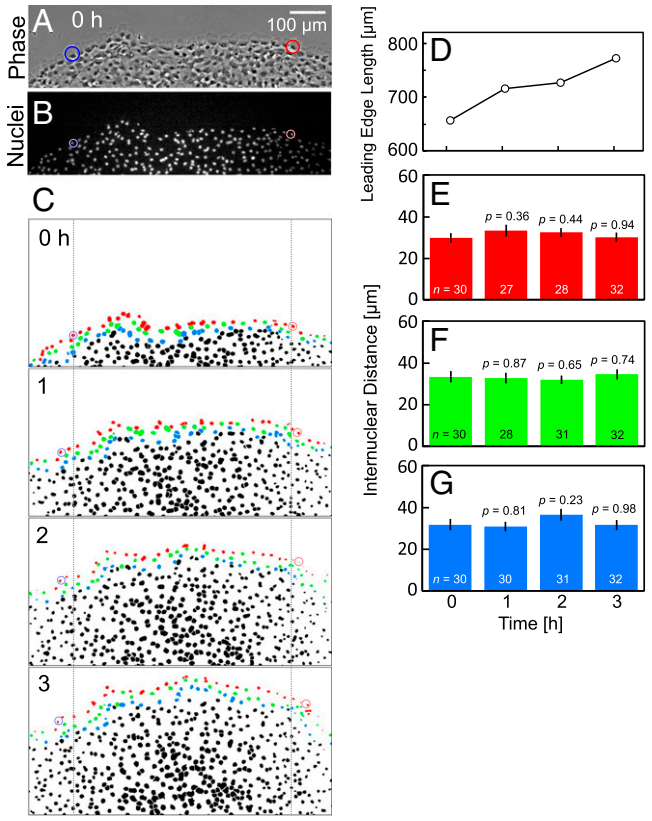

Fig. 2. Constant area size of the leader cells and the subsequent follower cells during the sheet's advance. (*A* and *B*) Phase-contrast image of a keratocyte sheet (*A*) and fluorescence image of nuclei of each cell (*B*). (*C*) Binarized sequential images of nuclei. In *A–C*, circled cells and nuclei with the same color indicate identical ones. They are moving outward from the area between the dotted lines in *C*. Red, yellow, and blue nuclei are those in the leader cells and the first and second row follower cells, respectively. (*D*) Time course of the leading-edge length between the two circled cells in *C*. (*E–G*) Average internuclear distance between adjacent leader cells, first and second row follower cells, respectively. There is no significant difference in the values of 1 to 3 h compared to those of 0 h in *E–G*. Error bars in *E–G* represent SEM. The *P* values were calculated using Student's *t* test. *A–G* are typical of three experiments.

course of the internuclear distance between adjacent leader cells at the leading edge (red dots in Fig. 2*C*) was measured based on the binarized sequential nucleus images in Fig. 2*C*. Although the length of the leading edge between the two leader cells (circled in blue and red in Fig. 2*C*) increased (Fig. 2*D*), the internuclear distances did not significantly change (Fig. 2*E*). The internuclear distances between the follower cells in the front and the second row (green and blue, respectively, in Fig. 2*C*) were also measured. In neither case did the distance significantly change (Fig. 2 *F* and *G*). These results clearly indicate that a change in the area of leader cells is not the cause of elongation of the leading edge.

The Number of Leader Cells is Increased by the Interruption of Single Follower Cells into the Leading Edge. Next, we examined whether or not the number of leader cells increases. Every third leader cell in the leading edge of a cell sheet was marked and their trajectories were traced for 3 h (Fig. 3*A* and Movie S3). As the sheet advanced, the number of cells between the marked cells increased (Fig. 3*B*). Cell numbers tend to increase consecutively at the same or close locations (*a-b*, *d-e*, and *g-h* in Fig. 3 *A* and *B*, and *SI Appendix*, *c-d* in Fig. S2*A*, *a-b*, and *f-g* in Fig. S2*B*, and arrows in Fig. S2 *C–E*). The total numbers of leader cells in the leading edge between two arbitrarily selected cells also increased in all 11 sheets (Fig. 3*C*, triangles; data made from Fig. 3*B*). On the other hand, the average cell width, the value obtained by dividing the leading-edge length by the number of cells, did not change (Fig. 3*D*).

To investigate how the number of leader cells increases, we used phase-contrast microscopy to observe the migration of individual cells around the leading edge (Fig. 3*E* and Movie S4). We found that a single follower cell (yellow arrows in Fig. 3*E*) interrupted between leader cells (asterisks in Fig. 3*E*), although no cell division could be seen. We also detected a stretched line (white arrows in Fig. 3*E*) emerging between the two leader cells before the interruption. The line then broke as the lamellipodium of the interrupting follower cell was extended. The lamellipodium extended faster after the line had disappeared (Fig. 3*F*). The breaking of this stretched line was confirmed with good reproducibility ($n = 11$). Three other examples are shown (*SI Appendix*, Fig. S3 *A–C* and Movie S5). This observation suggests that the single interrupting follower cells may mechanically push to break the actomyosin cables that stretch between two leader cells by the force of their protrusion. The next question is how single follower cells interpose themselves between two leader cells.

Contractile Forces of Actomyosin Cables between A Single Follower Cell and Two Adjacent Leader Cells Enable Interruption. First, to clarify whether the subsequent follower cells are pushing the interrupting follower cells, we measured the velocity of each migrating cell in an advancing cell sheet (Fig. 4 *A–C*). Unexpectedly, the leader cells in the leading edge migrated the fastest, and the further away from the leading edge, the slower the cell velocity was (Fig. 4 *B* and *C* and Movie S6). On the other hand, the directionality (defined as Euclidian distance divided by total distance traveled) of migrating cells in the sheet was almost the same from the leading edge to the rear of the sheet (*SI Appendix*, Fig. S4*A*) and was close to 1 (*SI Appendix*, Fig. S4*B*). These results suggest that the leader cells need to pull the follower cells behind to realize the overall migration of the sheet. If this is the case, not the follower cells but the leader cells should exert large traction forces in the direction opposite to that of migration.

We first compared the cell sheets between on the elastic substrate for traction force microscopy and on the coverslip. On the elastic substrate, F-actin and vinculin were shown in the lamellipodia in leader cells in the bottom optical section (*SI Appendix*, Fig. S5*A*). Actomyosin cables connected via cell-to-cell adhesions containing vinculin were shown at the boundary between the lamellipodium and the cell body of leader cells in the middle optical section (*SI Appendix*, Fig. S5*B*). These observations are just same as on the coverslip (Fig. 1 *I* and *J*). Velocity and directionality of the cell sheets also showed no significant difference between them (*SI Appendix*, Fig. S5 *C* and *D*).

Then, we measured the traction forces under the advancing cell sheets. The traction forces were mostly detected just beneath the lamellipodia of leader cells (Fig. 4 *D* and *E* and Movie S7). The direction of the forces was roughly opposite to the direction of the sheet advance. These results rule out the possibility that the follower cell closest to the leader cells is pushed into the leading edge by the follower cells behind it. Thus, the interruption mechanism in this study should differ from that of nonadherent leading edge of MDCK cells, which is driven by the posterior cell-proliferative pressure (29).

To investigate the roles of actomyosin cables and lamellipodial extension in the migration of the sheet, blebbistatin, a

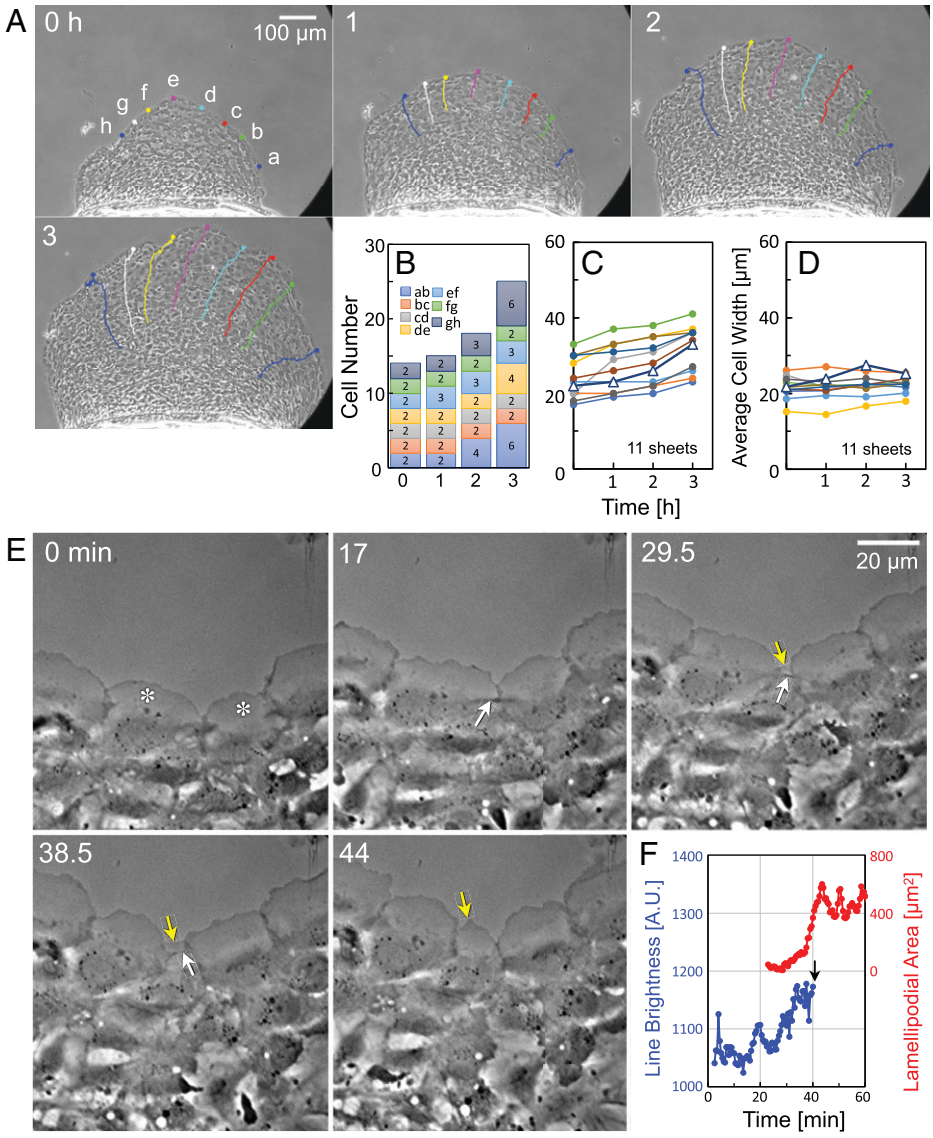

Fig. 3. Interruption of single follower cells into the leading edge. (*A*) Trajectories of eight (*a–h*) leader cells. Images in *A* are typical of 11 sheets. (*B*) The number of interval cells between the marked cells (*a–h*) in *A*. (*C*) The total numbers of leader cells between two arbitrarily selected cells from 11 sheets. (*D*) Average cell width of leader cells, calculated by dividing the values in Fig. 1*C* by the values in *C*. (*E*) Phase-contrast sequential images of a single follower cell interruption into the leading edge. First, between the two leader cells (asterisks at 0 min), a dark line appears and is stretched (white arrow at 17 min). Next, the tip of a lamellipodium extends beyond the line (yellow arrow in 29.5 min). The line then breaks (white arrow at 38.5 min), the leader cells separate, and the lamellipodia grow larger (yellow arrows at 44 min). Images in *E* are typical of 13 events from 9 sheets. (*F*) Time courses of the lamellipodial area of the interrupting cell and the brightness of the dark line in *E*. At 40.5 min (arrow), the line disappeared.

specific myosin II ATPase inhibitor, was added to the migrating sheets (*SI Appendix*, Fig. S6). Actomyosin cables entirely disappeared at 25 μM blebbistatin (*SI Appendix*, Fig. S6 *A* and *B*). Traction forces detected beneath the lamellipodia of leader cells dramatically decreased (*SI Appendix*, Fig. S6*C*). However, the sheet advanced, albeit at lower velocity and lower directionality (*SI Appendix*, Fig. S6 *D–F* and Movie S8), as reported in previous studies (35, 36). The sheet could no longer maintain the semicircular pattern during the migration of the sheet (*SI Appendix*, Fig. S6*D*), and the number of leader cells did not change (*SI Appendix*, Fig. S6*G*). These results indicate that not only the contraction of the actomyosin cables but also the other function (i.e., lamellipodial extension contributes to the advance of the sheet) and further suggest the following three possibilities. 1) The traction forces should be exerted primarily by the contraction of the actomyosin cables. 2) The leader cells should keep at optimal distances and directions from each other by the contractile forces of the actomyosin cables to maintain the semicircular pattern of the sheet. 3) Leading-edge tension due to the contraction of the actomyosin cables should contribute to the follower cell interruption. These possibilities need to be strictly demonstrated in the future, because blebbistatin inhibits not only the polymerization of actomyosin cables but also other functions related to myosin II ATPase.

Next, to clarify whether the interrupting cells operate independently, we measured the traction forces exerted by an interrupting follower cell and the cells surrounding it (Fig. 4*F* and Movie S9). At the beginning of the interruption, large traction forces were detected at the boundaries between the interrupting cell (black arrow at 0 min in Fig. 4*F*) and two leader cells on both sides of it. The regions where the large traction forces were detected (red area at 0 min in Fig. 4 *F*, *Lower*) were on the boundary between the lamellipodium and the cell body (yellow and gray lines at 0 min in Fig. 4*F*), where actomyosin

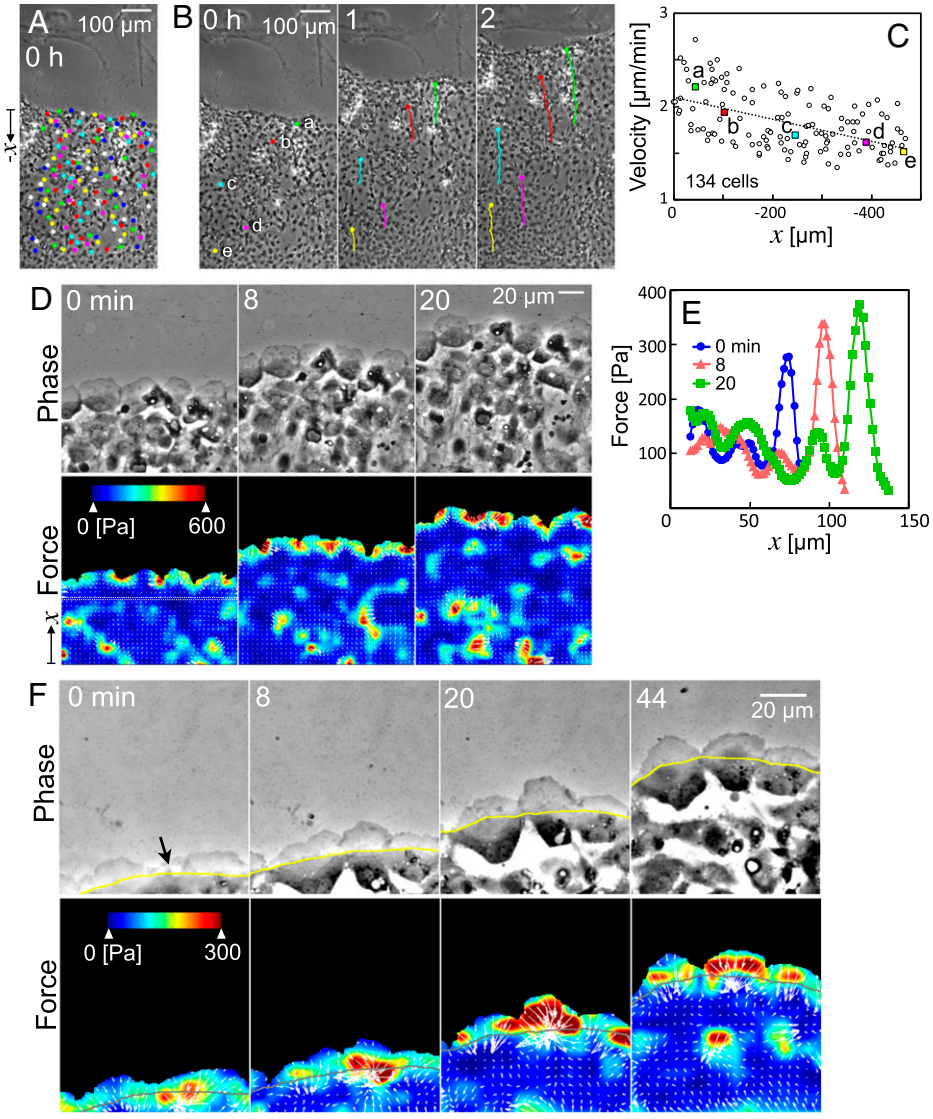

Fig. 4. Distributions of migration velocities and traction forces in the advancing sheet. (*A*–*C*) Comparison of cell-migration velocities in an advancing sheet. Velocities of dotted cells in *A* are shown in *C*. The trajectories of five selected cells are shown in *B*. Their velocities are indicated by the same-color squares in *C*. The *x* axis of *C* represents the distance from the leading edge at 0 h as a negative number. Straight dotted line in *C* is a regression line obtained by the least-squares method. *A*–*C* are typical of five sheets. (*D*) Traction forces exerted by an advancing keratocyte sheet. During the measurement, no follower cell interruption occurred. Large traction forces are shown under the lamellipodia of the leader cells in the direction opposite to the advancement of the sheet. Images in *D* are typical of eight sheets. (*E*) Average traction forces in the area every 1.6 μm in width (between two dotted lines in *D*). The *x* axis of *E* represents the distance from the bottom of each frame in *D*. (*F*) Traction force distribution around an interrupting follower cell (arrow in 0 min). The yellow lines in the phase images and the gray lines in the force images are on the boundary between the lamellipodium and the cell body where the actomyosin cables are present. At the beginning of the interruption (0 min), large traction forces (red area) were detected at the boundaries between the interrupting cell and two adjacent leader cells on the actomyosin cables. Images in *F* are typical of four sheets.

cables are present (36, 37, 40) (Fig. 1 *E*, *J*, and *K*). However, the directions of the forces were not parallel to the cables but toward the center of the interrupting cell (0 min in Fig. 4 *F*, *Lower*). The two large traction regions then fused (8 min in Fig. 4 *F*, *Lower*), and moved forward to the lamellipodium in the interrupting follower cell (20 and 44 min in Fig. 4 *F*, *Lower*). This distribution of traction forces after the end of the interruption is exactly the same as that in leader cells (Fig. 4 *D*, *Lower*). Occasionally, consecutive interruptions of multiple cells were detected at the same location (*SI Appendix*, Fig. S7), supporting the consecutive increase in the number of leader cells (*SI Appendix*, Fig. S2).

Our traction force measurements suggest that individual follower cells and the two adjacent leader cells are connected by newly emerging actomyosin cables, and the follower cells interrupt between the two leader cells by the contraction of the newly connected cables. If this is the case, to be able to complete the interruption, the original connection of actomyosin cables between leader cells needs to be broken.

New Actomyosin Cables Are Connected and Old Ones Are Broken. We captured the dynamics of the actomyosin cable reconnections during the interruption of a single follower cell (Fig. 5*A* and Movie S10). F-actin fluorescence, which discloses actomyosin cables, was visualized with HMRef (41) in a living cell sheet. The rectangle in 13.5 min in Fig. 5*A* is enlarged in Fig. 5 *B* and *C*. From the sequential images at 30-s intervals, narrow regions (the white rectangle in 18.5 min in Fig. 5*A*) were cropped and aligned sequentially to construct a kymograph (Fig. 5*D*). The two leader cells (asterisk at 0 min in Fig. 5 *A*, *Upper*) were connected by actomyosin cables (white arrow at 0 min in Fig. 5 *A*, *Upper*). A follower cell and the two leader

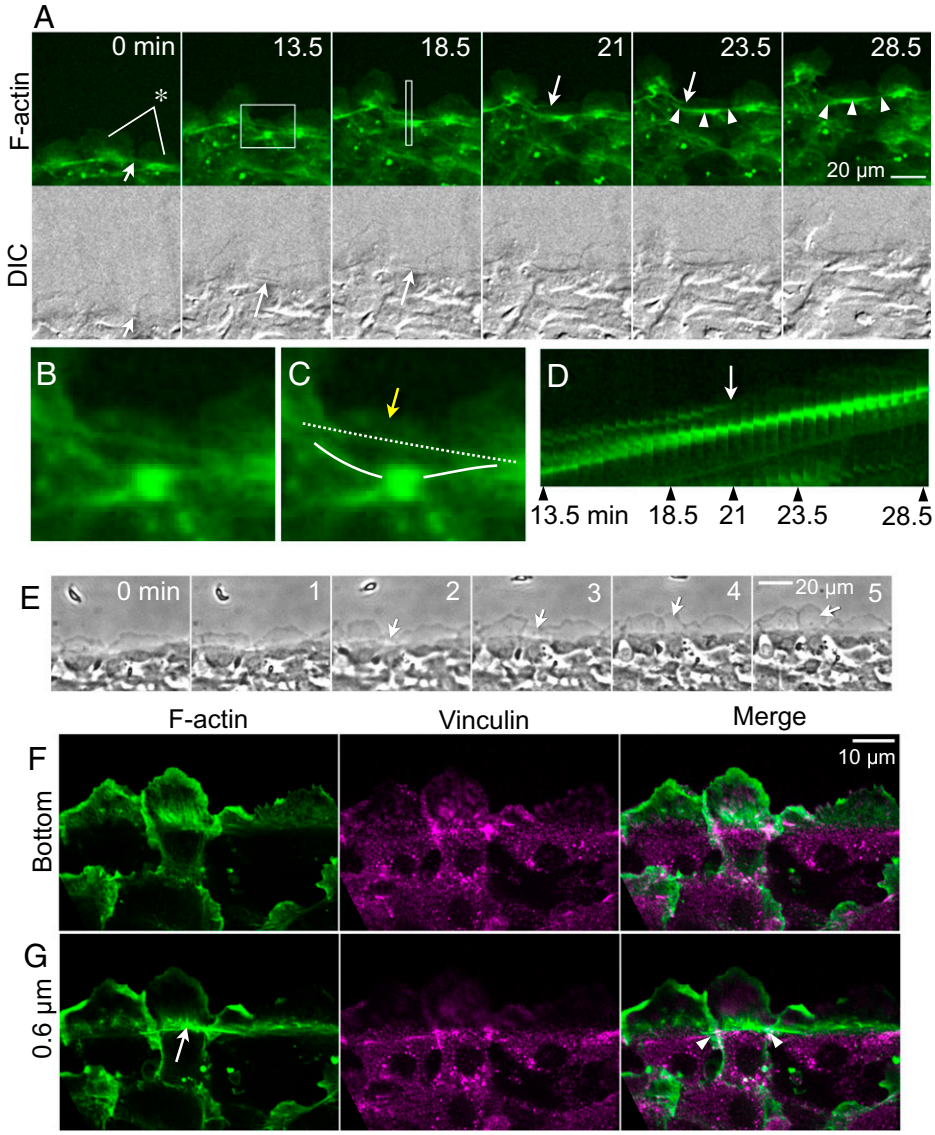

Fig. 5. Actomyosin cable reconnection by the interruption of a follower cell. (*A*) Live imaging of actomyosin cable reconnection. (*Upper*) F-actin visualized with HMRef. (*Lower*) DIC images. In the *Upper* F-actin images, white arrows at 0 min: original actomyosin cables between two leader cells (asterisk at 0 min); white arrows at 21 and 23.5 min: tip of the broken original actomyosin cables that had previously connected the two leader cells; arrowheads at 23.5 and 28.5 min: newly connected actomyosin cables. In the *Lower* DIC images, the white arrows show a stretched line corresponding to the original actomyosin cables. Images in *A* are typical of 11 interrupting cells from 8 sheets. (*B* and *C*) Enlarged (4.7×) images of the square in 13.5 min in *A*. *B* and *C* are the same photo. Original and newly connected actomyosin cables are traced with a dotted white line and solid white lines, respectively in *C*. Yellow arrow in *C*: lamellipodium protruding from the interrupting follower cell. (*D*) A kymograph constructed from image strips (white rectangles in 18.5 min in *A* from sequential images taken at 30-s intervals). The white arrow shows a fluorescence disappear due to breakage of the original actomyosin cables. (*E*) Interruption of a single follower cell into the leading edge. Arrows: an interrupting cell. Immediately after the last frame (5 min), the sheet was fixed and F-actin and vinculin staining were applied. (*F* and *G*) Bottom (*F*) and middle (*G*, 0.6 μm above the bottom) optical sections of a fixed keratocyte sheet: F-actin (green) and vinculin (magenta). Areas of colocalization of F-actin and vinculin appear white (*Right*). White arrow in *G*: newly formed actomyosin cables. White arrowheads in *G*: vinculin localization at the cell-to-cell adhesions on the actomyosin cables. Images in *F* and *G* are typical of five sheets.

cells were connected by new actomyosin cables at 13.5 min (white lines in Fig. 5*C*) that are distinct from the cables that had connected the two leader cells beforehand (white dotted line in Fig. 5*C*). The follower cell extended its lamellipodium (yellow arrow in Fig. 5*C*) beyond the actomyosin cables that had connected the two leader cells. The cables were then broken (arrow in Fig. 5*D*), probably by the migrations of leader cells that spread radially away from each other and the pushing force of the interrupting follower cell. The white arrows at 21 and 23.5 min in Fig. 5*A* indicate the right-hand end of the broken cables. The breaking of the original cables can also be detected in the DIC images (Fig. 5 *A*, *Lower*). Before breaking, but not after, a stretched line showing the actomyosin cables can be identified (white arrows in 0 to 18.5 min in Fig. 5 *A*, *Lower*) as shown in Fig. 3*E*. The follower cell began to behave as a leader cell, with new actomyosin cables (arrowheads at 23.5 and 28.5 min in Fig. 5*A*) connected to the leader cells on both sides. Breakage of the actomyosin cables between two leader cells due to interruption of a single follower cell was confirmed with good reproducibility ($n = 11$). The other three examples are shown (*SI Appendix*, Fig. S8 and Movie S11). In some cases (*SI Appendix*, Fig. S8*C*), the original actomyosin cables (*SI Appendix*, arrows in Fig. S8*C*) between the two leader cells move behind the new actomyosin cables (*SI Appendix*, arrowhead in Fig. S8*C*) before they are broken (between 21 and 31.5 min).

Finally, we checked at the molecular level whether the actomyosin cable connection between the interrupting follower cell

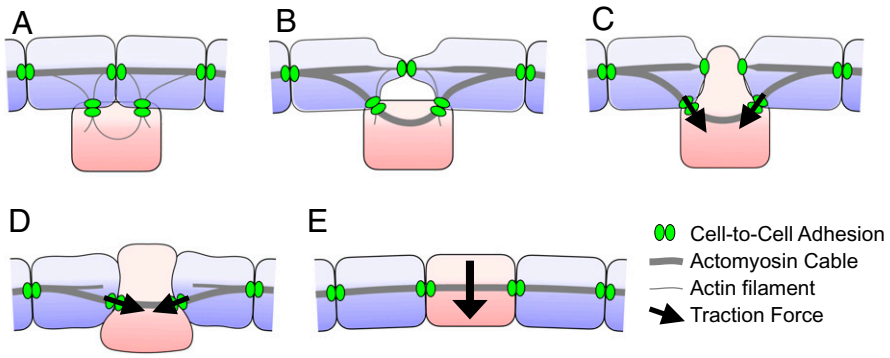

Fig. 6. A model for the leading-edge elongation in advancing epithelial cell sheets. (*A*) A follower cell (red) weakly connects to the two adjacent leader cells (blue) with cell-to-cell adhesions including vinculin. Only thin actin filaments extend from the adhesions into the cells. (*B*) The distance between the leader cells with low elasticity is widened by their radial migrations. The stretched thin actin filaments grow into actomyosin cables. (*C*) Using the connected actomyosin cables as a scaffold, contractile forces are exerted between the leader and follower cells (black arrows) and bring the follower cell forward. The follower cell extends its own lamellipodium between the two leader cells to break the original actomyosin cables. (*D*) The follower cell moves into the space between the leader cells. (*E*) Finally, the interrupted exfollower cell transforms into a leader cell that exerts traction forces beneath its lamellipodium in the opposite direction to that of the migration (black arrow). The light-colored area of each cell indicates its lamellipodium.

and its two adjacent leader cells could be completed in just a few tens of minutes after an interruption. Immediately after the interruption (Fig. 5*E* and Movie S12), the cell sheet was fixed, and F-actin was stained with Alexa 488 phalloidin (green in Fig. 5 *F* and *G*) and vinculin by immunofluorescence staining (magenta in Fig. 5 *F* and *G*). In the middle optical section (Fig. 5*G*), F-actin fluorescence (arrow in Fig. 5 *G*, *Left*) can be seen: evidence that actomyosin cables are already present in the interrupting follower cell. Colocalization of F-actin and vinculin appears white at the boundaries between the follower cell and the leader cells (arrowheads in Fig. 5 *G*, *Right*).

Discussion

Herein we propose a model for leading-edge elongation in advancing epithelial cell sheets (Fig. 6). A follower cell (red in Fig. 6*A*) connects to two adjacent leader cells using cell-to-cell adhesions, including vinculin. Only thin actin filaments extend from the adhesions into the cells. As the leader cells advance radially, the distance between the leader cells with low elasticity is widened (Fig. 6*B*). The stretched thin actin filaments grow into actomyosin cables. Using the connected actomyosin cables as scaffolds, contractile forces are exerted between the leader and follower cells, and the forces bring the follower cell forward (black arrows in Fig. 6*C*). The follower cell extends its own lamellipodium between the two leader cells, breaking the original actomyosin cables. Then, the follower cell moves into the space between the leader cells (Fig. 6*D*). Finally, the interrupting follower cell transforms into a leader cell that exerts traction forces with its lamellipodium in the direction opposite to that of the migration of the sheet (black arrow in Fig. 6*E*).

Coexistence of cellular protrusion, such as extension of lamellipodia, and actomyosin purse-string behavior in leading-edge cells have been reported not only in keratocytes but also in other epithelial cells, such as adult mouse corneas (10) and dorsal closure of *Drosophila* embryos (14, 15). *Drosophila* embryos that have lost the actomyosin cables display an irregular and misshapen leading edge (42). In the case of keratocyte sheets too, the actomyosin cables are likely to contribute to the coordinated movement of leader cells, because the actomyosin cableless leading edge could not maintain its shape (*SI Appendix*, Fig. S6*D*). Consecutive or intermittent interruption of follower cells (*SI Appendix*, Figs. S2 and S7) may continue at the low elastic regions of leading edge until the elasticity is restored. If this is the case, keratocyte sheets will enlarge while maintaining its shape.

The migration velocity of cells in the sheet was fastest for leader cells at the leading edge of the sheet and slower toward the rear (Fig. 4*C*). This fact means that only the cells that interpose themselves into the leading edge show special behavior that distinguishes them from normal follower cells. There are two possible ways for this special behavior to be realized. Certain follower cells may be able to move forward faster than the many other follower cells. Alternatively, despite there being no difference in any of the follower cells, a trigger may induce certain leader cells to pull up an adjacent follower cell. In this case, the pulling forces between the follower cell and the two leader cells detected as the traction forces (Fig. 4*F*) may be generated by the leader cells, the follower cell, or both cells. Identification of follower cells that begin interruption and identification of signals that cause the leader cells to begin pulling an adjacent follower cell will be an interesting future subject of research.

Correlation between the geometry of the epithelium leading edge with the gap-closure mechanisms (i.e., whether the local curvature of the leading edge induces either lamellipodial extension or actomyosin cable assembly) has recently been investigated. Cells tend to form lamellipodia at straight or convex edges of the cell sheets, but are more likely to form actomyosin cables at concave edges (18, 43–45). Actomyosin cable-switching found by Wei et al. (29) occurs at concave edge. A follower cell enters the leading edge due to posterior cell-proliferative pressure, while an adjacent leader cell moves away from the leading edge. The authors concluded that the actomyosin cable-switching empowers the purse-string contraction for gap closure. On the other hand, keratocyte sheets have a vast and convex leading edge (Fig. 1*A*). Leader cells in the leading edge have both a large lamellipodium and at the same time are connected to each other with purse-string–like actomyosin cables (Fig. 1) (36). Since the leading edge moved forward even if the actomyosin cables were disassembled by blebbistatin treatment (*SI Appendix*, Fig. S6*D*), the driving force for sheet outgrowth is likely not only the contraction of actomyosin cables but also the extension of the lamellipodia.

Fish scales play a role in protecting the body from mechanical stimuli. When a fish receives a mechanical stimulus, the scales detach instead of damaging the internal body. Since the scales reach several millimeters in size, the wounds are shallow but large. Such wounds would occur frequently in fish.

Reepithelialization of skin wounds in fish is extremely rapid (30). The wound healing rate reaches 500 μm/h (46). This is 50 times faster than in human skin (47). It was shown that only 8% of the cells on a sheet were labeled by BrdU, a marker of proliferating cells, and that inhibition of cell division by mitomycin C had no effect on sheet advancement (40), suggesting that the cell proliferation is unlikely to be the cause of leading-edge extension. The leading-edge extension by the interruptions of follower cells into the leading edge demonstrated in this study may contribute to this rapid wound healing. In fact, at the leading edge of the healing epidermis, flat keratocytes have been observed, although undetected connection with the actomyosin cables yet (46).

In a single keratocyte, stress fibers are arranged in the cell body perpendicular to the direction of cell advance (48). By contracting its stress fibers, the cell exerts traction forces on the substrate at both the left and right ends of the cell body (49). The directions of these traction forces are toward the center of the cell, that is, almost perpendicular to the direction of cell advance. On the other hand, the leader cells of keratocyte sheets exert traction forces below the lamellipodia in the opposite direction to the cell advance (Fig. 4*D*). These results suggest that the actomyosin cables that connect the leader cells of keratocyte sheets become stress fibers when the cell collective returns to single cells, and that the migration mechanics are different between leader cells of keratocyte sheets and single keratocytes, although they both have lamellipodia.

Finally, we have shown here the connecting and breaking of actomyosin cables among two leader cells and an interrupting follower cell in epithelial cell sheets. Actomyosin cable remodeling takes place both in the nonadhesive gap closure (29) and in the leading edge driven by adhesive lamellipodial extension in this study, while the mechanisms are quite different. It may therefore be commonly seen in collective cell migration. Although collective cell migration has been widely studied, our data offer new insights into its mechanisms.

Materials and Methods

Cell Culture. Keratocyte sheets from the scales of African cichlids (*M. lombardoi*) were cultured as previously described (48). The detailed method is described in *SI Appendix*.

Fixed Cell Staining. Fixed cell staining was performed according to the methods described previously (49). The detailed method is described in *SI Appendix*.

Confocal Microscopy. Fluorescence images of live or fixed cells were detected using an inverted microscope (Ti; Nikon) equipped with a laser confocal scanner unit (CSU-X1; Yokogawa) and an electron multiplying CCD camera (DU897; Andor) through a 100× objective lens (CFI Apo TIRF 100× H/1.49; Nikon). The CCD had 512 × 512 active pixels and the pixel size through the objective was 0.13 μm.

Epi-Fluorescence Microscopy. In some cases, fluorescence images of live cells were detected using an inverted microscope (Ti; Nikon) equipped with a laser (Sapphire 488-20; Coherent) as an excitation light source, dichroic mirror (FF493_574-Di01; Semrock), absorption filter (SC-64; Fujifilm), and CCD camera (ORCA-ER-1394; Hamamatsu Photonics) through a 10× objective lens (CFI Plan Fluor DLL 10×; Nikon) or a 20× objective lens (CFI Plan Fluor DLL 20×; Nikon). The CCD's active pixels are 1,344 × 1,024 and the pixel size through the objective was 0.64 (10×) or 0.32 μm (20×).

Traction Force Microscopy. Traction force microscopy was performed according to the methods described previously (50), with minor modifications. The detailed method is described in *SI Appendix*.

Fluorescent Staining of Nuclei in Advancing Cell Sheets. DRAQ5 (BioStatus) was dissolved at 5 mM in DMSO and then diluted 2,000 times with culture medium. This DRAQ5 medium was then added to the chamber, to the bottom of which the cell sheets had adhered, immediately after removal of the culture medium. After 10 min, the DRAQ5 medium in the chamber was replaced with the culture medium. The cell sheets in the chamber were used for experiments without external DRAQ5.

The number of cell rows from the leading edge of the cell of interest (Fig. 2*C*) was determined by a self-made macro (*SI Appendix*) in ImageJ from the fluorescence of the nucleus.

Fluorescent Staining of Filamentous Actin in Advancing Cell Sheets. HMRef, a novel probe for F-actin developed by Ueno and colleagues (41), was dissolved at 1 mM in DMSO and then diluted 4,000-fold with culture medium. This HMRef medium was then added to the chamber, to the bottom of which the cell sheets had adhered, immediately after removal of the culture medium. After 10 min, the cell sheets in the chamber were used for experiments without removal of the HMRef medium.

Blebbistatin Treatment. Blebbistatin treatment was performed according to the methods described previously (48), with minor modifications. The detailed method is described in *SI Appendix*.

Data Availability. All raw data generated in this study are available on Zenodo, https://zenodo.org/record/6350749.

ACKNOWLEDGMENTS. This study was supported by The Ministry of Education, Culture, Sports, Science, and Technology Kakenhi Grants 21K15055 (to C.O.), 17K07366, 19H04935, 20H03227, and 21K19228 (to Y.I.), and 16H06574 (to T.U.); and by Japan Society for the Promotion of Science Core-to-Core Program JPJSCCA20170007 (to Y.U.).

1. P. Friedl, D. Gilmour, Collective cell migration in morphogenesis, regeneration and cancer. *Nat. Rev. Mol. Cell Biol.* **10**, 445–457 (2009).
2. R. Mayor, S. Etienne-Manneville, The front and rear of collective cell migration. *Nat. Rev. Mol. Cell Biol.* **17**, 97–109 (2016).
3. P. Martin, J. Lewis, Actin cables and epidermal movement in embryonic wound healing. *Nature* **360**, 179–183 (1992).
4. M. T. Abreu-Blanco, J. M. Verboon, S. M. Parkhurst, Cell wound repair in *Drosophila* occurs through three distinct phases of membrane and cytoskeletal remodeling. *J. Cell Biol.* **193**, 455–464 (2011).
5. X. Soto *et al.*, Inositol kinase and its product accelerate wound healing by modulating calcium levels, Rho GTPases, and F-actin assembly. *Proc. Natl. Acad. Sci. U.S.A.* **110**, 11029–11034 (2013).
6. M. Tamada, T. D. Perez, W. J. Nelson, M. P. Sheetz, Two distinct modes of myosin assembly and dynamics during epithelial wound closure. *J. Cell Biol.* **176**, 27–33 (2007).
7. S. R. K. Vedula *et al.*, Mechanics of epithelial closure over non-adherent environments. *Nat. Commun.* **6**, 6111 (2015).
8. W. M. Bement, P. Forscher, M. S. Mooseker, A novel cytoskeletal structure involved in purse string wound closure and cell polarity maintenance. *J. Cell Biol.* **121**, 565–578 (1993).
9. W. Wood *et al.*, Wound healing recapitulates morphogenesis in *Drosophila* embryos. *Nat. Cell Biol.* **4**, 907–912 (2002).
10. Y. Danjo, I. K. Gipson, Actin 'purse string' filaments are anchored by E-cadherin-mediated adherens junctions at the leading edge of the epithelial wound, providing coordinated cell movement. *J. Cell Sci.* **111**, 3323–3332 (1998).
11. S. Grasso, J. A. Hernández, S. Chifflet, Roles of wound geometry, wound size, and extracellular matrix in the healing response of bovine corneal endothelial cells in culture. *Am. J. Physiol. Cell Physiol.* **293**, C1327–C1337 (2007).
12. M. Reffay *et al.*, Interplay of RhoA and mechanical forces in collective cell migration driven by leader cells. *Nat. Cell Biol.* **16**, 217–223 (2014).
13. A. Brugués *et al.*, Forces driving epithelial wound healing. *Nat. Phys.* **10**, 683–690 (2014).
14. A. Jacinto *et al.*, Dynamic actin-based epithelial adhesion and cell matching during *Drosophila* dorsal closure. *Curr. Biol.* **10**, 1420–1426 (2000).
15. M. J. Redd, L. Cooper, W. Wood, B. Stramer, P. Martin, Wound healing and inflammation: Embryos reveal the way to perfect repair. *Philos. Trans. R. Soc. Lond. B Biol. Sci.* **359**, 777–784 (2004).
16. E. Maniou *et al.*, Hindbrain neuropore tissue geometry determines asymmetric cell-mediated closure dynamics in mouse embryos. *Proc. Natl. Acad. Sci. U.S.A.* **118**, e2023163118 (2021).
17. P. Rørth, Collective cell migration. *Annu. Rev. Cell Dev. Biol.* **25**, 407–429 (2009).
18. E. Anon *et al.*, Cell crawling mediates collective cell migration to close undamaged epithelial gaps. *Proc. Natl. Acad. Sci. U.S.A.* **109**, 10891–10896 (2012).
19. M. Poujade *et al.*, Collective migration of an epithelial monolayer in response to a model wound. *Proc. Natl. Acad. Sci. U.S.A.* **104**, 15988–15993 (2007).
20. S. R. K. Vedula *et al.*, Emerging modes of collective cell migration induced by geometrical constraints. *Proc. Natl. Acad. Sci. U.S.A.* **109**, 12974–12979 (2012).
21. T. Omelchenko, J. M. Vasiliev, I. M. Gelfand, H. H. Feder, E. M. Bonder, Rho-dependent formation of epithelial "leader" cells during wound healing. *Proc. Natl. Acad. Sci. U.S.A.* **100**, 10788–10793 (2003).

22. L. Petitjean *et al.*, Velocity fields in a collectively migrating epithelium. *Biophys. J.* **98**, 1790–1800 (2010).
23. M. Vishwakarma *et al.*, Mechanical interactions among followers determine the emergence of leaders in migrating epithelial cell collectives. *Nat. Commun.* **9**, 3469 (2018).
24. B. Ladoux, R.-M. Mège, Mechanobiology of collective cell behaviours. *Nat. Rev. Mol. Cell Biol.* **18**, 743–757 (2017).
25. M. Vishwakarma, J. P. Spatz, T. Das, Mechanobiology of leader-follower dynamics in epithelial cell migration. *Curr. Opin. Cell Biol.* **66**, 97–103 (2020).
26. S. Begnaud, T. Chen, D. Delacour, R.-M. Mège, B. Ladoux, Mechanics of epithelial tissues during gap closure. *Curr. Opin. Cell Biol.* **42**, 52–62 (2016).
27. L. Capuana, A. Boström, S. Etienne-Manneville, Multicellular scale front-to-rear polarity in collective migration. *Curr. Opin. Cell Biol.* **62**, 114–122 (2020).
28. R. Riahi *et al.*, Notch1-Dll4 signalling and mechanical force regulate leader cell formation during collective cell migration. *Nat. Commun.* **6**, 6556 (2015).
29. Q. Wei *et al.*, Actin-ring segment switching drives nonadhesive gap closure. *Proc. Natl. Acad. Sci. U.S.A.* **117**, 33263–33271 (2020).
30. L. Sveen, C. Karlsen, E. Ytteborg, Mechanical induced wounds in fish–A review on models and healing mechanisms. *Rev. Aquacult.* **12**, 2446–2465 (2020).
31. K. Keren *et al.*, Mechanism of shape determination in motile cells. *Nature* **453**, 475–480 (2008).
32. J. A. Theriot, T. J. Mitchison, Actin microfilament dynamics in locomoting cells. *Nature* **352**, 126–131 (1991).
33. C. A. Wilson *et al.*, Myosin II contributes to cell-scale actin network treadmilling through network disassembly. *Nature* **465**, 373–377 (2010).
34. A. Mogilner, E. L. Barnhart, K. Keren, Experiment, theory, and the keratocyte: An ode to a simple model for cell motility. *Semin. Cell Dev. Biol.* **100**, 143–151 (2020).
35. J. S. Martinez, J. B. Schlenoff, T. C. S. Keller 3rd, Collective epithelial cell sheet adhesion and migration on polyelectrolyte multilayers with uniform and gradients of compliance. *Exp. Cell Res.* **346**, 17–29 (2016).
36. T. Morita, A. Tsuchiya, M. Sugimoto, Myosin II activity is required for functional leading-edge cells and closure of epidermal sheets in fish skin ex vivo. *Cell Tissue Res.* **345**, 379–390 (2011).
37. J. L. Rapanan, K. E. Cooper, K. J. Leyva, E. E. Hull, Collective cell migration of primary zebrafish keratocytes. *Exp. Cell Res.* **326**, 155–165 (2014).
38. D. Mohammed *et al.*, Substrate area confinement is a key determinant of cell velocity in collective migration. *Nat. Phys.* **15**, 858–866 (2019).
39. R. Farooqui, G. Fenteany, Multiple rows of cells behind an epithelial wound edge extend cryptic lamellipodia to collectively drive cell-sheet movement. *J. Cell Sci.* **118**, 51–63 (2005).
40. R. Matsumoto, M. Sugimoto, Dermal matrix proteins initiate re-epithelialization but are not sufficient for coordinated epidermal outgrowth in a new fish skin culture model. *Cell Tissue Res.* **327**, 249–265 (2007).
41. T. Takagi *et al.*, Discovery of an F-actin-binding small molecule serving as a fluorescent probe and a scaffold for functional probes. *Sci. Adv.* **7**, eabg8585 (2021).
42. A. Ducuing, S. Vincent, The actin cable is dispensable in directing dorsal closure dynamics but neutralizes mechanical stress to prevent scarring in the *Drosophila* embryo. *Nat. Cell Biol.* **18**, 1149–1160 (2016).
43. T. Chen *et al.*, Large-scale curvature sensing by directional actin flow drives cellular migration mode switching. *Nat. Phys.* **15**, 393–402 (2019).
44. J. K. Klarlund, Dual modes of motility at the leading edge of migrating epithelial cell sheets. *Proc. Natl. Acad. Sci. U.S.A.* **109**, 15799–15804 (2012).
45. A. Ravasio *et al.*, Gap geometry dictates epithelial closure efficiency. *Nat. Commun.* **6**, 7683 (2015).
46. A. Quilhac, J. Y. Sire, Spreading, proliferation, and differentiation of the epidermis after wounding a cichlid fish, *Hemichromis bimaculatus*. *Anat. Rec.* **254**, 435–451 (1999).
47. R. Iglesias-Bartolome *et al.*, Transcriptional signature primes human oral mucosa for rapid wound healing. *Sci. Transl. Med.* **10**, eaap8798 (2018).
48. C. Okimura, A. Taniguchi, S. Nonaka, Y. Iwadate, Rotation of stress fibers as a single wheel in migrating fish keratocytes. *Sci. Rep.* **8**, 10615 (2018).
49. T. Nakata, C. Okimura, T. Mizuno, Y. Iwadate, The role of stress fibers in the shape determination mechanism of fish keratocytes. *Biophys. J.* **110**, 481–492 (2016).
50. C. Okimura, Y. Sakumura, K. Shimabukuro, Y. Iwadate, Sensing of substratum rigidity and directional migration by fast-crawling cells. *Phys. Rev. E* **97**, 052401 (2018).